GAs for aerodynamic shape design II: multiobjective optimization and multi-criteria design

D. Quagliarella, A. Vicini
C.I.R.A., Centro Italiano Ricerche Aerospaziali
Via Maiorise — 81043 Capua (Italy)

Abstract

The lecture focuses on multi-objective genetic algorithms with hybrid capabilities, and on their application to multi-criteria design problems. A short introduction to multi-point aerodynamic shape design is given, and the advantages of a multi-objective optimization approach to this problem are outlined. The introduction of basic concepts of multi-objective optimization is followed by the description of a multiple objective genetic algorithm. Some techniques for efficiency improvement are introduced; in particular, the gradient based technique for hybrid optimization is extended to multi-objective design problems. Application examples are reported related both to single and multi-element airfoil design in high-lift conditions, and to transonic wing design.

1 Introduction

The aerodynamic design problem can be defined as the determination of the shape of bodies that satisfy design goals and constraints that can be either of aerodynamic or geometrical and structural nature [1].

Design problems are often characterized by several conflicting requirements that have to be satisfied at the same time.

For example, the main goal of the aerodynamic design of a wing for a transport aircraft is to minimize the drag in cruise condition, but this is not enough to obtain an efficient transport wing. Several additional criteria must be met such as buffet boundary high enough to permit cruising at design lift coefficients, no pitch-up tendencies near stall, no unsatisfactory off-design performances [2]. Furthermore, several non-aerodynamic requirements have to be taken into account, such as weight and structural constraints.

On the other hand, the main goal of a high lift system could appear simpler at a first glance, as, in this case, the objective of the aerodynamic design is to achieve maximum lift without massive flow separation [3]. As a matter of fact, the problem is even more complicated, because a high-lift system has a strong impact on wing weight, complexity and costs and its integration into a wing requires a true multidisciplinary approach.

When conflicting requirements have to be satisfied at the same time, the usual approach is to reduce the multiobjective problem into a classical single objective one. Here,

instead, will be described a different technique based on direct solution of the multiobjective problem. Basic concepts and definitions of multiobjective optimization are given in the following, and an approach to its resolution based on genetic algorithms is developed.

2 Multiple objective optimization

In mathematical terms, a Multi-objective Optimization Problem (MOP) may be defined as:

$$\min_{\mathbf{x} \in X} \boldsymbol{f}(\mathbf{x}) \tag{1}$$

where $\boldsymbol{f} \triangleq (f_1(\mathbf{x}), \ldots, f_n(\mathbf{x}))$ is a vector of m real valued objective functions, $\mathbf{x}$ is a vector of n decision variables and

$$X \triangleq \{\mathbf{x} \mid \mathbf{x} \in \mathbf{R}^n, \ \ g_i(\mathbf{x}) \leq 0, \ i = 1, \ldots, p, \ \ h_j(\mathbf{x}) = 0, \ j = 1, \ldots, q \ \text{ and } \ \mathbf{x} \in S\}$$

is the feasible solution set, $g_i(\mathbf{x})$ and $h_j(\mathbf{x})$ are real valued functions representing the constraints and S is a subset of $\mathbf{R}^n$ representing any other form of constraint (for example a discrete set). The ideal solution of such a problem is a point where each objective function assumes its best possible value. This ideal solution in most cases does not exist due to the conflicting nature of the objectives. Hence, solutions to these problems have to be a compromise between the various requirements. An usual approach to find a compromise solution is the reduction of the multiobjective problem into a classical single objective one through a weighted combination of the objective functions. The drawback of this technique is that the solution obtained depends on the arbitrary choice of the relative weights assigned to the objectives. It would be interesting, instead, to find all the best compromise solutions available, and choose 'a posteriori' the solution best fitted to the problem. This approach naturally leads to a new definition of optimality: a feasible solution to a multiobjective optimization problem is said Pareto optimal, or non dominated, if, starting from that point in the design space, the value of any of the objective functions cannot be improved without deteriorating at least one of the others.

All feasible solutions to a multi-objective problem can thus be classified into dominated and non dominated (Pareto optimal) solutions, and the set of globally non dominated solutions of a multi-objective problem is called Pareto front. These are all possible alternative solutions to the problem, which meet the requirements at different level of compromise. In this way, the arbitrary choice regarding the weights to attribute to each different design criteria is avoided. Consequently, the first step in the solution of a multi-objective problem consists in finding (or approximating) this set or a representative subset. Afterwards the decision maker's preference may be applied to choose the best compromise solution from the generated set.

The natural ordering of vector valued quantities is basic for Pareto optimality. To define the notion of domination let $\mathbf{f} = (f_1, \ldots, f_m)$ and $\mathbf{g} = (g_1, \ldots, g_m)$ be two real-valued vectors of m elements; $\mathbf{f}$ is partially less than $\mathbf{g}$ (in symbols $\mathbf{f} <_{\mathsf{p}} \mathbf{g}$) if:

$$\forall i \in 1, \ldots, m, \ \ f_i \leq g_i, \ \text{ and } \ \exists i : f_i < g_i \tag{2}$$

If $\mathbf{f} <_{\mathsf{p}} \mathbf{g}$, we say that $\mathbf{f}$ dominates $\mathbf{g}$. Consequently, a feasible solution $\mathbf{x}^*$ is said a Pareto optimal solution of the problem in equation 1 if and only if it does not exist another $\mathbf{x} \in X$ such that $\boldsymbol{f}(\mathbf{x}) <_{\mathsf{p}} \boldsymbol{f}(\mathbf{x}^*)$.
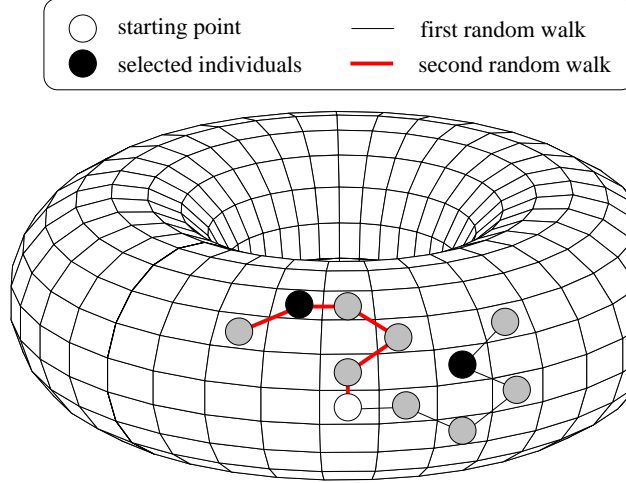
Figure 1: Random walk selection scheme

Two different strategies are possible for generating Pareto optimal solutions. The first one consists in the reduction to a Single-objective Optimization Problem (SOP) in parametric form, so that the solution of the SOP with given values of the parameters, under certain conditions, belongs to the Pareto front; changing the parameters of the SOP leads the solution to move on the front. In the second one, the MOP is solved with a direct approach using the dominance criteria, so that a set of Pareto optimal solutions is developed simultaneously. The main advantage of the first strategy is that SOPs are, generally, very well studied problems and many efficient methods are available to solve them. On the other hand, it has to be pointed out that some reduction strategies do not guarantee a complete equivalence between the original MOP and the resulting parametric SOP, when some conditions on the feasible set and on the objective functions are not satisfied. Consequently, some Pareto optimal solutions may never be discovered using this reduction approach [4]. Furthermore, even when the reduction scheme allows a complete equivalence of the problems, it may be necessary to solve a great number of SOPs to have a representative subset of the Pareto front. Two possible ways of defining the equivalent SOPs are the weighting approach and the constraint approach. Details on these methods can be found in [5]; their basic features are also summarized in [6].

Solving directly the MOP has the advantage of finding a representative subset of the Pareto front in one shot. Genetic algorithms can be used to effectively solve a MOP using the dominance criteria to drive the evolution of the population. The characterizing feature of a multiobjective GA is thus the introduction of the Pareto criteria in the method used for individuals selection [7]; by selecting individuals in the reproduction phase according to the domination criteria, a set of non dominated solutions can be developed.

Various approaches are possible in the implementation of a multiple objective genetic algorithm [7, 8]. The technique followed here is a direct extension of the single-objective GA obtained by directly introducing the dominance criteria in the selection mechanism. This has been accomplished by selecting (at least a part of) the elements appointed for reproduction using a random walk operator; in this case, the elements selected are not the best fit ones, but the locally non dominated among those met in the walk. In more detail, the random walk selection is performed in two phases on a population distributed

over a toroidal landscape (see figure 1).

In the first phase, a starting point in the landscape is chosen at random, and the locally non dominated individuals met in a random walk of assigned number of steps from that starting point are marked as possible candidates of being the first parent; the second parent candidates are selected in the same way in a successive random walk from the same starting point.

In the second phase the parents are chosen from the two sets of candidates. If a set has more than one candidate parent, then a secondary ranking criterion must be introduced. Various choices are possible. The simplest one may be the minimization (or maximization) of the distance from the starting point (measured along the walk). Following this rule, the first (or, respectively, the last) element of the candidate set is chosen. A more sophisticate ranking criterion may be the distance (in the objective space) of the candidate parent from the current Pareto front. Another possible rule may be the minimum value of one of the objectives.

A sort of extension of the elitist strategy to multiobjective optimization may also be adopted by randomly selecting an assigned percentage of parents from the current set of non dominated solutions. Moreover, the possibility of selecting a specified percentage of individuals through a roulette-wheel operator – acting on one of the objectives of the optimization problem randomly chosen – has been introduced. This increases selection pressure towards the minima of the objectives of the problem considered individually, improving the behavior of the algorithm in locating the extrema of the Pareto front. The amount of parents selected by roulette-wheel can possibly be decreased as evolution proceeds.

Hybridization can be used to improve the genetic algorithm performance also in the case of multiple objective optimization. A hybrid operator based on gradient computation has been here introduced in the multi-objective GA.

The gradient operator is, by its nature, capable of improving scalar objective functions; when applied to multiobjective problems, it is therefore necessary to transform the MOP into an equivalent SOP. The weighting approach has been chosen here to obtain the equivalent SOP. The objective function passed to the gradient operator is obtained as a weighted linear combination of the problem objectives, i.e. as $obj = \alpha obj_1 + (1 - \alpha)obj_2$, where $\alpha \in [0, 1]$, in the case of $n = 2$. The approach followed here, however, does not try to transform the MOP into an equivalent parametric SOP. Rather, it fixes the parameters of the SOP so that only one solution is found rather than a non-dominated set. This however is not a limit, because the gradient based operator acts like a local improvement operator. Therefore the weight α can be chosen at random or assigned explicitly to give greater importance to one of the objectives.

Concerning the methods for the selection of the appointed individuals, an extension of the strategies adopted for single-objective problems is considered; The choice of the elements to be fed into the gradient search may be done following three different schemes characterized by a different selection pressure:

1. a number of elements, determined by an assigned probability, is selected from the current Pareto front;

2. a number of individuals, determined by an assigned probability, is chosen using a selection operator from the current population;
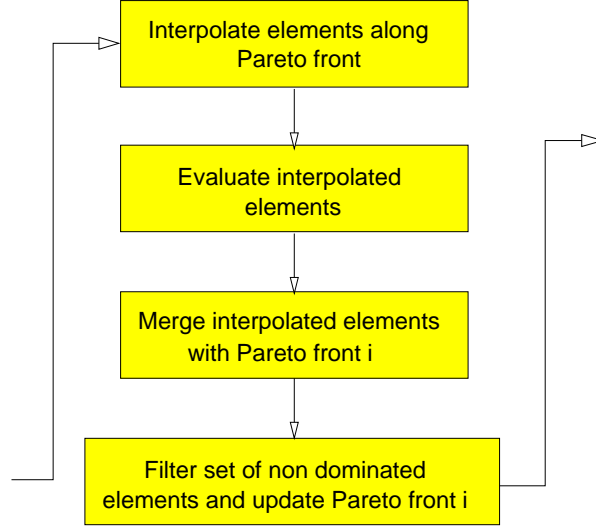
Figure 2: Interpolation technique for two-objectives problems.

3. a number of individuals, determined by an assigned probability, is chosen at random from the current population.

Another method for improving the quality of Pareto fronts is here illustrated, and its application has been demonstrated in some of the examples presented. It is an interpolation technique and it has been implemented for two-objective optimization problems; this technique consists in what follows:

1. All the couples of adjacent individuals along the front current Pareto front at generation i $(\mathcal{P}_i')$ are considered, and, if their distance (measured in the objectives plane) is higher than a specified percentage of the average distance between adjacent elements of the Pareto front, a new individual is generated by linear interpolation of
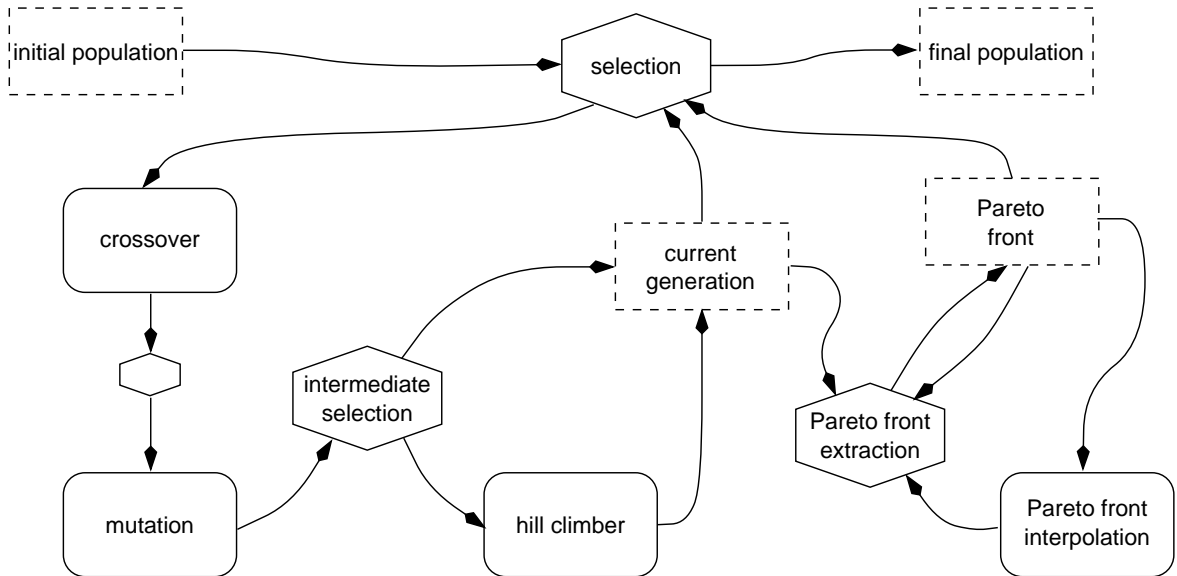

Figure 3: Scheme of the hybrid multi-objective genetic algorithm.

their design variables;

2. after their evaluation, all the new individuals thus generated are merged with the current Pareto front set $\mathcal{P}_i'$, and the new set of non dominated individuals $\mathcal{P}_i$ is extracted.

A flow chart of the resulting algorithm is illustrated in figure 2. This procedure has two positive effects: the first one is the enrichment of the Pareto front at the end of each generation, as many of the elements obtained through interpolation belong to the non dominated set; the second advantage is the exploitation of the first one, and it is obtained when an elitist strategy is adopted by selecting some of the individuals in the reproduction phase from the current Pareto front. The combination of these two effects allows to improve the approximation of the Pareto front with more and better distributed individuals.

A scheme which summarizes the hybrid multi-objective genetic algorithm with Pareto front interpolation is reported in figure 3 and it is explained in the following:

1: Initialization
A population G_0 of m elements is generated at random or by mutation over a given starting point, and evaluated with respect to each of the n objective functions.

2: Selection, Crossover and Mutation
The elements to mate are selected, recombined through the crossover and mutation operator, and the obtained offspring is evaluated and stored into a new intermediate generation G_i'.

3: Application of the gradient based operator
If active at the current generation, some elements are chosen from G_i' according to the adopted strategy, and gradient is applied. The obtained elements substitute the old ones and a new current generation G_i is obtained.

4: Pareto front extraction
After new generation G_i is completed, it is merged with the current Pareto front ($\mathcal{P}_{i-1}$), and the new set of non dominated individuals (updated Pareto front, $\mathcal{P}_i$) is extracted and stored.

5: Pareto front interpolation
If interpolation is active, the interpolated solutions are added to the current front $\mathcal{P}_i$ and the non dominated elements are again extracted and stored in $\mathcal{P}_i$.

6: Termination
If the maximum number of allowed generations or the ideal solution have been reached, then the process stops, else continue from step **2**.

3 Transonic airfoil design

The reported problem consists in the reduction of wave drag of a RAE 2822 airfoil while keeping the corresponding pitching moment under control. It is an example of the use of

multiobjective optimization to solve constrained design problems. The objective functions to be minimized are:

$$\begin{aligned} o_1 &= c_{dw}/c_l^2 \\ o_2 &= c_m^2 \end{aligned} \tag{3}$$

The design point is $M = 0.78$, $c_l = 0.75$ and maximum thickness is fixed equal to that of the initial geometry. The constraint on lift coefficient is satisfied by letting the flow solver find the angle of attack that produces the desired lift, whereas the thickness of the airfoil is scaled to the desired value after each geometry modification. The geometry is represented using 12 modification functions, y_i:

$$y = y_o + \sum_{i=1}^{N} x_i \, y_i \tag{4}$$

A full potential flow solver is used for fitness evaluation [9]. The GA parameters are reported in table 1.

Variables encoding	8 bit
Selection	3 step random walk
Crossover	one-point, $p_c = 1$
Mutation	bit level, $p_m = 0.02$
Population size	100
Generations	100

Table 1: Genetic algorithm parameters used for the transonic airfoil design problem.

Gradient operator is used, on average, on one element per generation, chosen at random from the Pareto front; the run stopped at generation 86 to establish the comparison for the same total number of objective function evaluations. From the analysis of the fronts reported in figure 4 it can be seen how the hybrid algorithm gave a front characterized by solutions of higher quality and more uniformly distributed.

4   High-lift airfoil design

The first example reported is a lift coefficient maximization problem at $M = 0.2$ and $R = 8000000$ and control on pitching moment. The objective functions to be minimized are therefore:

$$\begin{aligned} o_1 &= 1/c_l^2 \\ o_2 &= k(\underline{c}_m - c_m)^2 \end{aligned} \tag{5}$$

where $\underline{c}_m = -0.27$. The angle of attack, at which the configuration has to be optimized, is chosen to be $5°$. A constraint is imposed on the maximum thickness of the airfoil:

$$t = 9.7\% \tag{6}$$

The initial two-component airfoil can be modified only in its upper front part; flap rotation and translation are allowed. A total of 13 design variables has been used (10 modification function + 3 degrees of freedom for the flap).
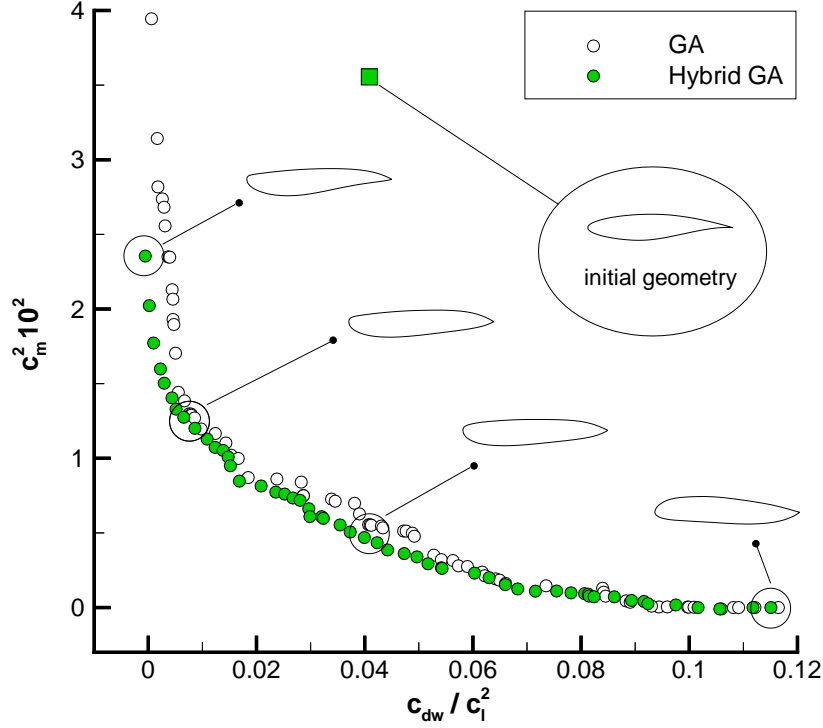
Figure 4: Pareto fronts obtained for the constrained transonic airfoil design problem.

The flow solver here used for high-lift configurations is an Euler+boundary layer interactive flow solver. The external solver is based on a streamline Euler discretization scheme and it is coupled to an integral boundary layer based on a multi-layer velocity profile representation (Drela's MSES code [10]).

A population of 32 individuals evolved for 40 generations; 8 bits were used for variable encoding; mutation at bit level with a probability of 2% and extended intermediate crossover with 100% activation probability were used. Figure 5 reports the final Pareto front and some intermediate ones.

An airfoil belonging to the middle part of the final front was chosen and the comparison of its c_p distribution and shape with respect to the original configuration are reported in figures 6 and 7, respectively.

The chosen airfoil has lift coefficient and pitching moment coefficient equal to 2.135 and -0.315 respectively, which correspond to 0.219 and 0.40 objective function values.

The second example is related to a dual point design solved through a multiobjective approach in which the first objective controls the lift coefficient in high lift ($M = 0.20, R = 8000000$), and the second one the wave drag coefficient in transonic cruise ($M = 0.85$). The objective functions are therefore:

$$\begin{aligned} o_1 &= 1/c_l^2 \\ o_2 &= k c_{dw} \end{aligned} \tag{7}$$

The thickness constraint has been set at $t = 9.5\%$, no control is imposed on the pitching moment. The modification functions operate on the whole airfoil, and the high lift devices are modified following the blending method described in part I. A full potential flow solver is used for cruise configuration evaluation [9].
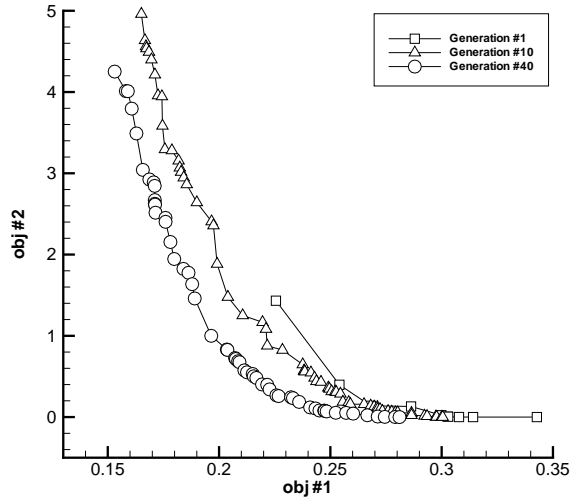
8

Figure 5: Final and intermediate Pareto fronts for the c_l maximization problem with constrained c_m.

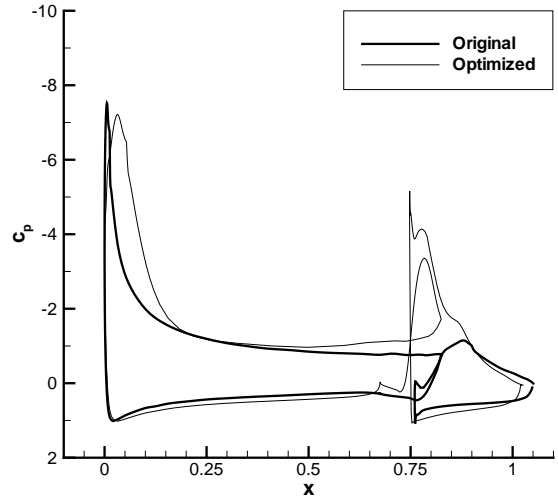

Figure 6: c_p comparison for the c_l maximization with constrained c_m.

Figure 7: Airfoil comparison for the c_l maximization with constrained c_m.

A total of 33 modification function have been used, and flap rotation and translation is allowed.

A population of 40 individuals evolved for 20 generations; 8 bits were used for variable encoding; mutation at bit level with a probability of 2% and extended intermediate crossover with 100% activation probability were used. Figure 8 reports the final Pareto front and some intermediate ones.

The airfoil of the final front with better transonic performance was chosen. Figure 9 reports its shape, along with the initial one, in the open and closed configurations. The ordinate scale is enlarged in order to allow a better comparison.

For this airfoil, the lift coefficient c_l is equal to 2.18 in the first design point, while the wave drag coefficient c_{dw} in the second design point is equal to 0.0099.

5 Applications to wing design

5.1 Wing geometry parameterization

Both wing planform and section shapes can be modified by the optimization procedure. In the application presented, wing planform has been kept trapezoidal, so that all geometric characteristics vary linearly from the root section to the tip. A total of 6 design variables
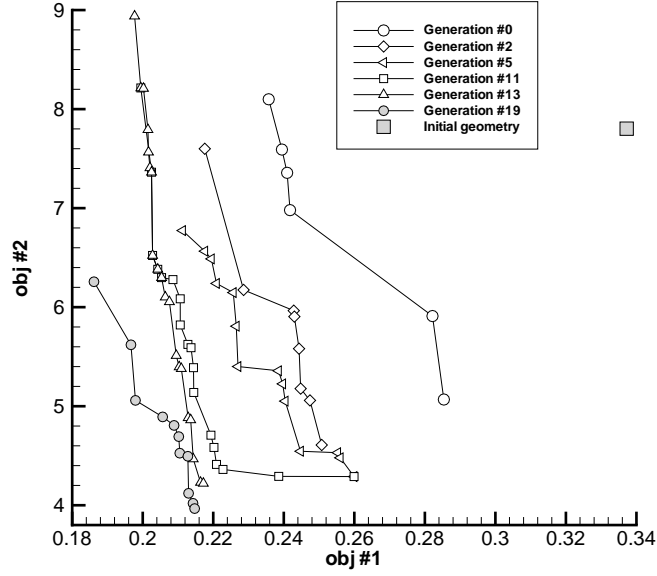
Figure 8: Final and intermediate fronts related to the c_l maximization in high-lift with control on c_{dw} in cruise condition example.
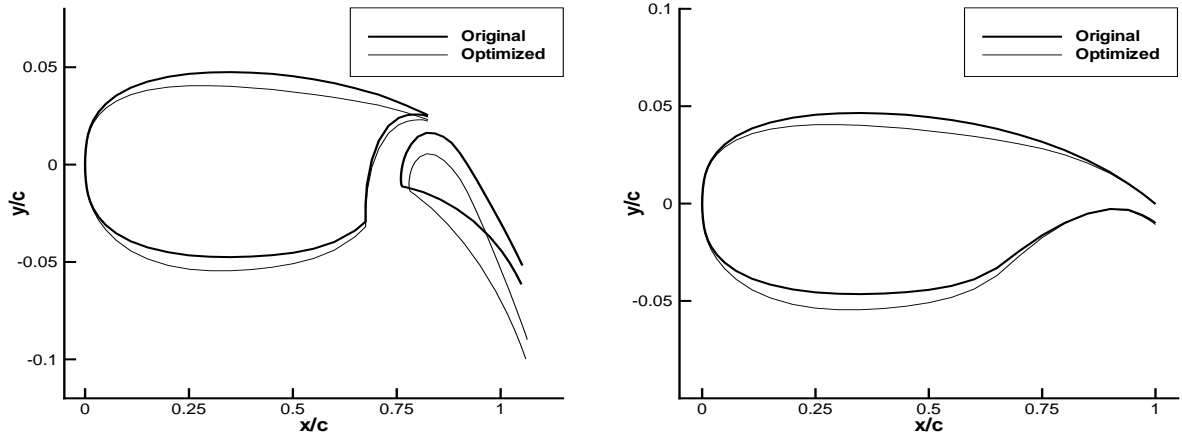

Figure 9: Open and closed airfoil configuration comparison for the dual design point problem (c_l-c_{dw}).

can be used: 4 of these act directly on the wing planform, namely the taper ratio λ, the sweep angle at 25% of the chord Λ, the aspect ratio AR and the twist angle θ; moreover, the (percent) thickness at the wing root and tip have also been included among the design parameters. The geometry modifications are made in such a way that the wing surface is kept constant, so that the average wing loading is not changed during optimization.

The wing geometry is assigned through a number of spanwise "control" sections, as discussed in part I of this work.

5.2   Wing planform design

As anticipated, the design of a transonic wing planform will first be illustrated; the design has been accomplished by minimizing inviscid aerodynamic drag, which combines

10

induced and wave drag, and structural weight, at a given Mach number $M = 0.84$ and lift coefficient $c_L = 0.3$. The starting geometry chosen is the ONERA M6 wing[11]; this wing has an aspect ratio AR=3.8, a leading edge sweep $\Lambda = 30°$, a taper ratio $\lambda = 0.562$, and is untwisted. The shape of the airfoil is symmetrical, with a maximum thickness of about 9.8 % chord. A total of 5 design variables have been used; in table 2 the initial values of the design parameters are reported together with the prescribed allowable ranges. The thickness at the wing tip has been fixed at the original value $t/c \mid_t = 9.8$ %. For all the cases that will be described, the constraint on the lift coefficient has been satisfied by using the angle of attack as a free parameter, and letting the flow solver adjust it to meet the desired lift value.

The wing twist is distributed symmetrically between the root and the tip, so that a twist angle θ corresponds to an increase of local incidence of $\theta/2$ at the tip, and a decrease of $\theta/2$ at the root. The wing weight is computed using the algebraic equation of Torenbeek [12]; this equation combines analytical and empirical (statistical) methods, and has sensitivity and accuracy adequate for its use in preliminary design.

Individuals selection has been carried out through a 2 step random walk, with one-point crossover ($p_c = 1$) and bit mutation ($p_m = 0.1$), and a population of 16 individuals was let evolve for 10 generations.

The Pareto front obtained using the Pareto interpolation technique previously described is reported in figure 10 (where W_o and c_{Do} are the values of the original M6 wing), together with the planform of a few wings corresponding to the indicated positions along the front; the front is populated by 123 individuals. In the same picture also the Pareto front computed without the described interpolation technique is illustrated. In this case, 20 generations have been carried out, so that the two cases are compared approximately for the same total number of objective function evaluations; it can be seen how, in the latter case, a much coarser representation of the Pareto front is obtained (43 individuals).

In figure 11 the values of the design parameters of the solutions belonging to the Pareto front are shown as a function of aerodynamic drag. It is interesting to observe how the variation of each design parameter along the front is non linear; in particular, "peaks" of some of the design variables can be found in correspondence of "valleys" of others. The distributions are nevertheless piecewise linear, which explains why also a linear interpolation between two elements on the Pareto front is likely to belong, in turn, to the Pareto front.

design variable	initial value	allowable range
λ	0.562	[0.2 , 0.8]
Λ	30.0	[15 , 36]
θ	0.0	[-10 , 10]
AR	3.8	[3.5 , 4.2]
$t/c \mid_r$ %	9.8	[8 , 14]

Table 2: Design parameters for the wing planform optimization.

Problem #	$t/c\%$	twist	Mach	c_L	c_D	c_M	γ_{TE}	L.E. radius
1	9.8%	no	0.84	0.3	minimize	$\geq$-0.135	$\geq 10°$	free
2	9.8%	yes	0.84	0.3	minimize	$\geq$-0.135	$\geq 10°$	free
3	9.8%	no	0.84	0.3	minimize	$\geq$-0.135	$\geq 10°$	$\geq 1\%$ chord
4	9.8%	yes	0.84	0.3	minimize	$\geq$-0.135	$\geq 10°$	$\geq 1\%$ chord

Table 3: Formulation of the design problems for the M6 section optimization.

5.3 Wing section optimization

The design problem here presented consists in the minimization of (inviscid) drag for the ONERA M6 wing, at the design point $M = 0.84$, $c_L = 0.3$. The wing planform shape and the maximum thickness of the wing sections have been kept constant in the optimization process. Two geometrical constraint are introduced as penalty functions and act as a filter, by assigning a very high value to the objective function of those geometries which violate them, and skipping the aerodynamic analysis. The first geometrical constraint on the minimum allowable trailing edge angle (γ_{TE}) is used to avoid unfeasible geometries. The second one controls the leading edge radius to avoid undesirable off design performances. The pitching moment coefficient is controlled introducing an additional objective function. The twisted and untwisted cases are treated separately. The formulation of these design problems is summarized in table 3.

The first objective function is c_D/c_L^2 (to account for small variations of the lift coefficient around the design value).

The constraint on the maximum thickness of the wing sections, so as to maintain it at the same value of the original geometry, is imposed by scaling the sections to the desired thickness after each geometry modification.

The wing has been assigned using 4 spanwise "control" sections, at the positions $\eta = 0$, 0.33, 0.66 and 1.0. A total of 12 design variables have been used for the wing sections modification.

The pitching moment coefficient of the ONERA M6 wing at the design point is $c_M = -0.1315$ (evaluated using the full-potential flow model); thus, the considered constraint $c_M \geq -0.135$ corresponds to a maximum allowable decrease of about 2.5%.

The second objective function is hence $obj_2 = (c_M - \tilde{c}_M)^2$. The value $\tilde{c}_M = -0.130$ has been used; in this way, the solutions on the final Pareto front will be characterized by pitching moment coefficients in the range from approximately $\tilde{c}_M$ to a lower value corresponding to the minimum drag solutions. Two separate runs have been carried out by allowing or not the wing twist to be modified; the shape of the wing sections has been kept constant in the spanwise direction. The parameters of table 4 have been used for the genetic algorithm. In figure 12 the solutions belonging to the final Pareto fronts (problems 1–4) are illustrated; it must be noted that the solutions are not reported in the objectives plane, but directly in the $c_D - c_M$ plane, which explains why their distribution doesn't look exactly as a Pareto front.

It is now possible to choose a solution with the desired characteristics among those obtained; the aerodynamic coefficients of the minimum drag solutions which satisfy the constraint on pitching moment are reported in table 5. Figure 13 shows the drag rise

Selection	Random-Walk, 3 steps
Crossover	Extended Intermediate Recombination
P_c	1
Mutation	Word
P_m	0.05
Pop size	48

Table 4: genetic algorithm parameters for the two-objective wing section optimization.

curves at $c_L = 0.3$ of these wings compared to the original wing. The twisted wing, though characterized by lower drag at the design Mach number, shows a higher drag at lower Mach numbers (drag creep) respect to the untwisted wing.

It can be seen that, in the case of the untwisted solution, the decrease in aerodynamic drag is approximately 45 drag counts, with the pitching moment coefficient within the acceptable value. On the other hand, with the twisted solution a decrease in aerodynamic drag of approximately 54 drag counts is obtained, and the pitching moment coefficient is even reduced with respect to the initial value. In figures 14 and 15 the pressure distributions over the original and optimized wings are shown. When the wing is allowed to twist. it is possible to see how the intensity of the shock is reduced, while its position is to some extent anticipated in the outboard portion of the wing. Finally, in figures 16 and 17 the modified airfoil shapes are illustrated.

As can be seen from table 5, considering that the constraint on the pitching moment doesn't allow the optimizer to change the camber of the wing section very much, the final geometries in both cases are characterized by a significant reduction of the leading edge radius. This can be an unacceptable modification, as it may lead to unsatisfactory off design performances, in particular regarding high lift conditions (c_L^{MAX} of the clean wing). For this reason, the optimization procedure as described before has been repeated for the untwisted and twisted cases introducing an additional constraint on the leading edge radius, so that this could not be reduced to values lower than 1% of the local chord. It may be observed from figure 12 how the solutions on these Pareto fronts are similar to those obtained without the leading edge radius constraint at the low drag end of the fronts, whereas they are characterized by higher drag values in the low pitching moment region of the fronts. Considering the same constraint $c_M > -0.135$, the characteristics of the solutions that can be extracted from these fronts are reported as solution 3 and 4 in table 5.

The drag penalty of these solutions with respect to the corresponding ones without constraints on the leading edge radius is approximately 6.9 drag counts for the untwisted case, and 6.5 in the twisted one.

Figures 18 and 19 illustrate the pressure distributions over the original and optimized wings, whereas the corresponding geometries are illustrated in figures 20 and 21. When the wing is twisted, the position of the shock wave is slightly anticipated, but its intensity is reduced.

Problem	α	c_L	c_D	c_{Di}	c_{Dw}	c_M	θ	r_{LE}
M6 wing	3.3167	0.3000	0.01369	0.00700	0.00670	-0.13151	0.0	1.50%
1	3.4558	0.3000	0.00918	0.00700	0.00219	-0.13476	0.0	0.88%
2	2.8994	0.3002	0.00830	0.00731	0.00099	-0.12970	-4.09	0.37%
3	3.3823	0.3000	0.00987	0.00700	0.00288	-0.13475	0.00	1.14%
4	2.6742	0.3000	0.00895	0.00748	0.00147	-0.13237	-5.88	1.03%

Table 5: Aerodynamic coefficients of the optimized wings.
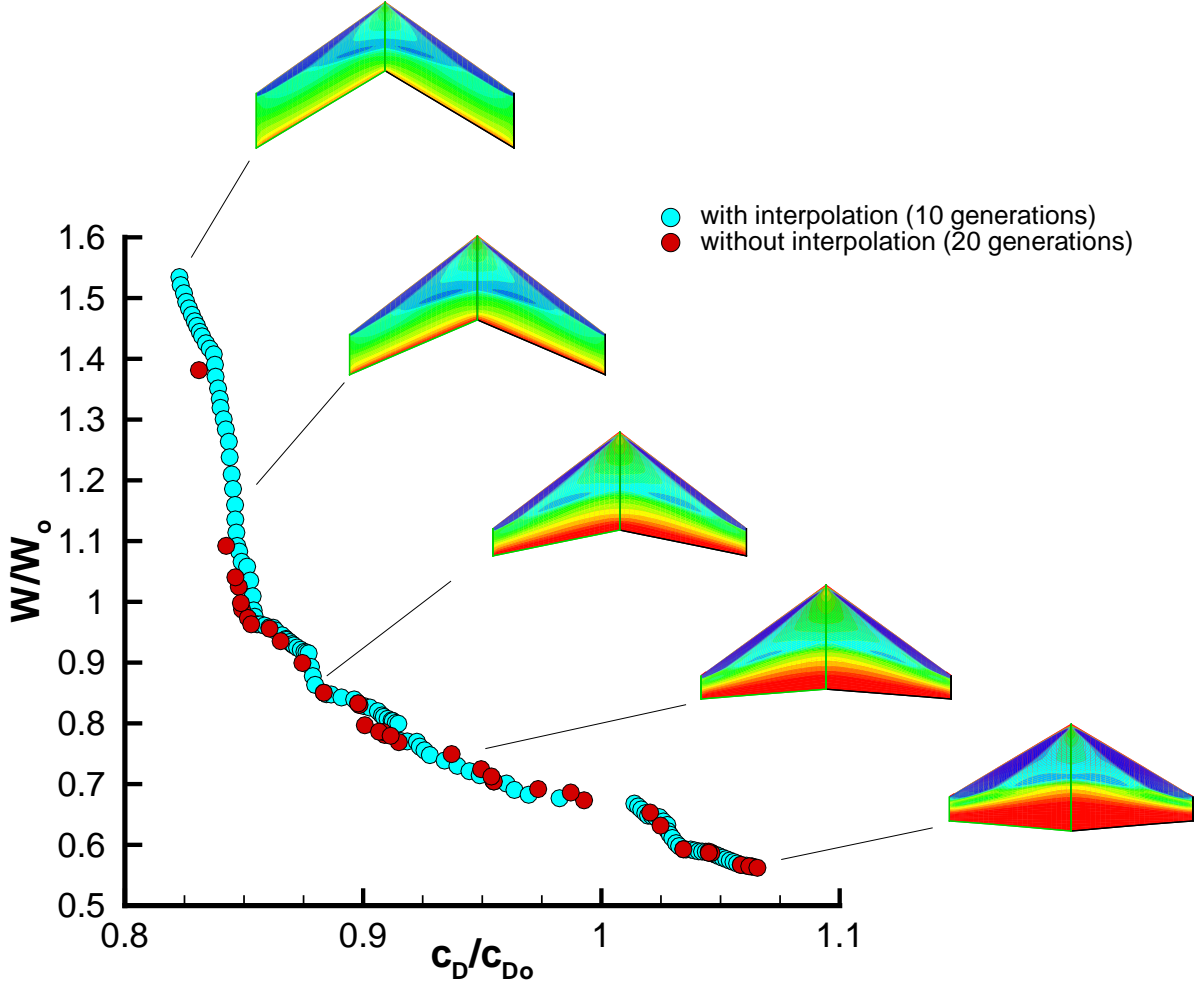
Figure 10: Pareto fronts obtained for the wing planform design problem

5.4 Three-objective wing section design

Another problem is finally presented with a second design point at higher Mach and lower lift coefficient in which control on aerodynamic drag is required. The optimization
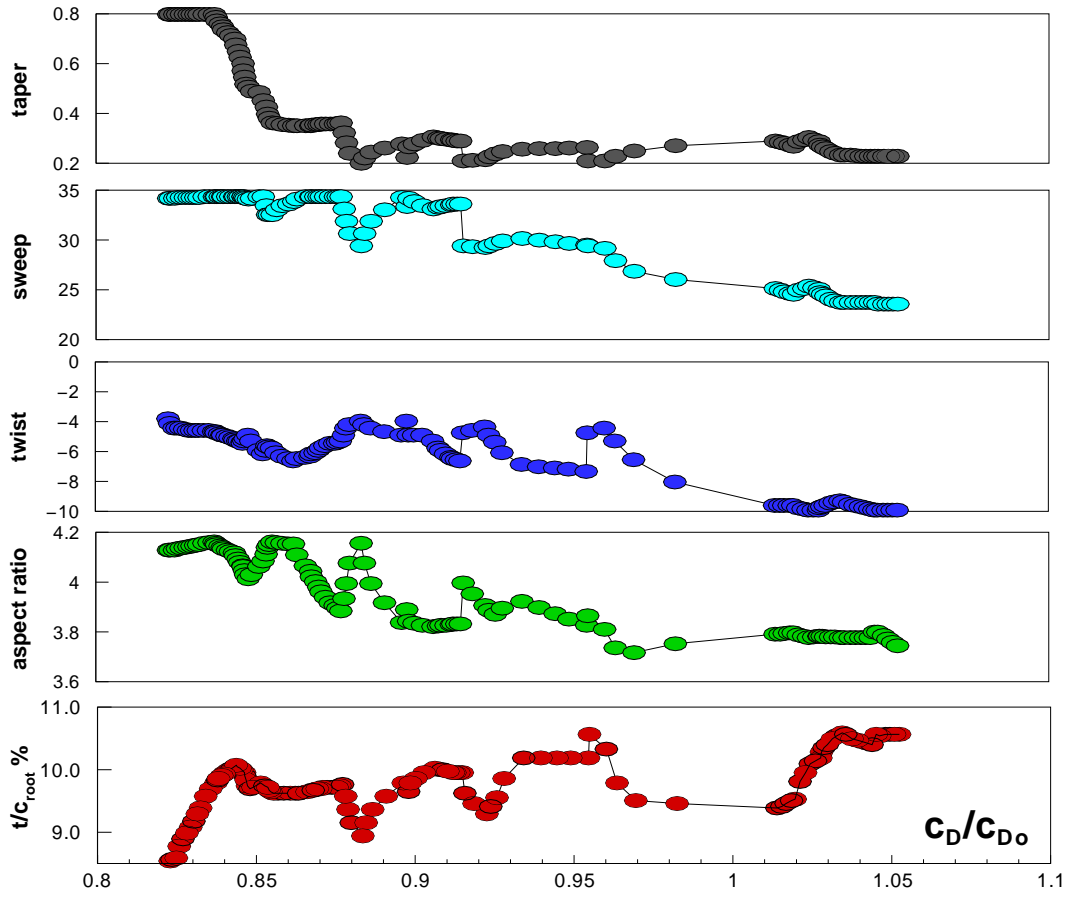
Figure 11: Values of the design parameters of the wing planforms belonging to the front
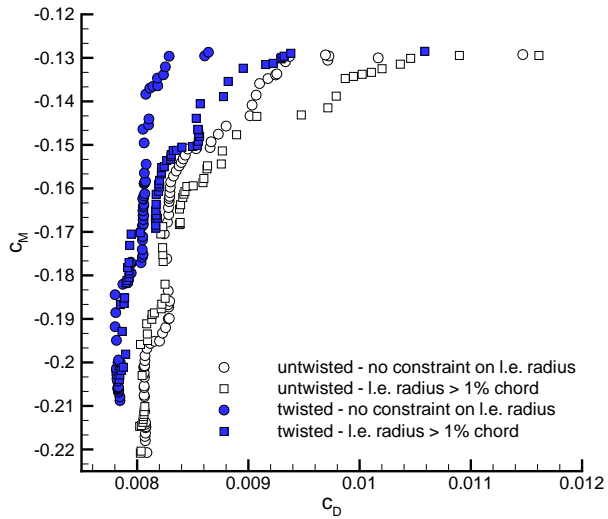
Figure 12: Pareto fronts for the wing sections design problems 1–4, reported in the C_D-C_M plane.
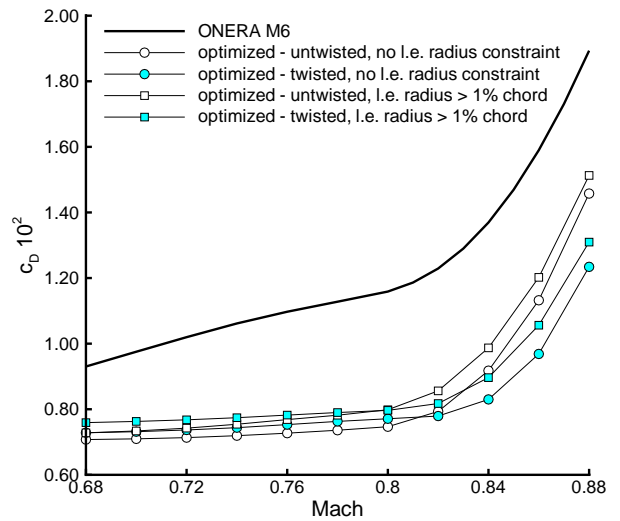
Figure 13: Drag rise curves at the design lift coefficient of the optimized wings with and without the constraint on leading edge radius.

15
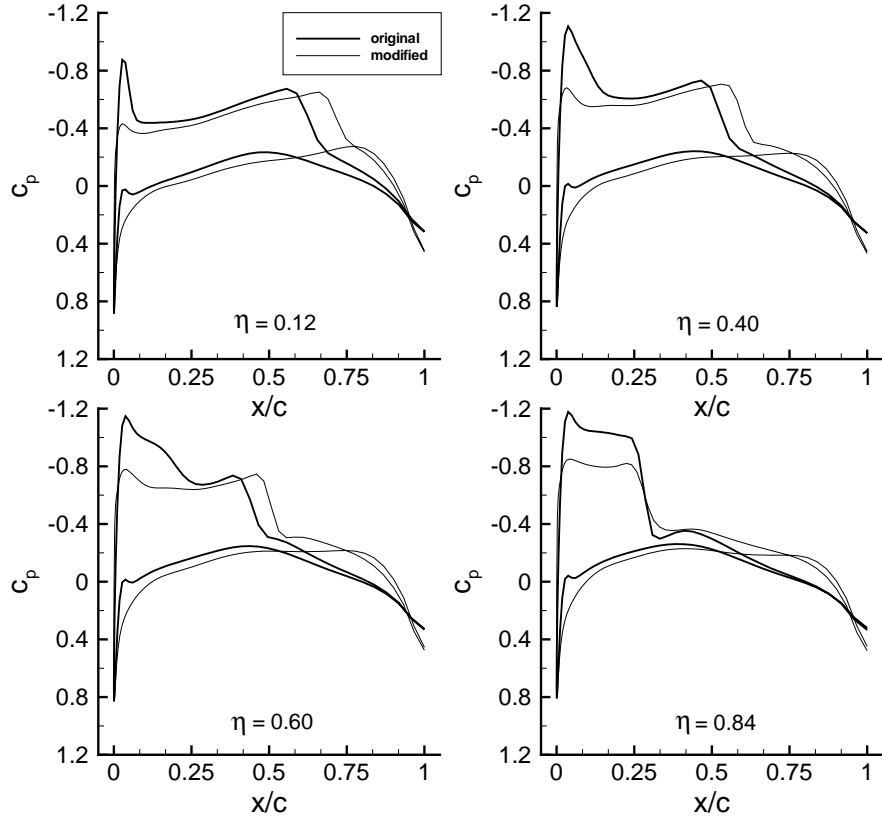
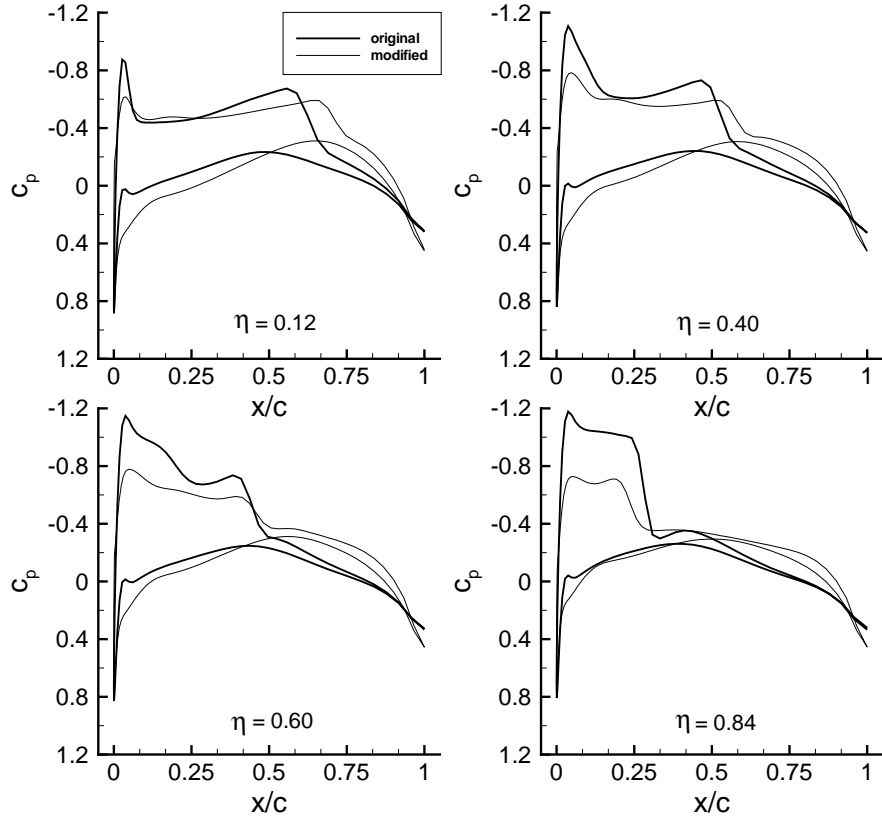Figure 14: Pressure coefficient distributions on the original and optimized (untwisted) wings

Figure 15: Pressure coefficient distributions on the original and optimized (twisted) wings
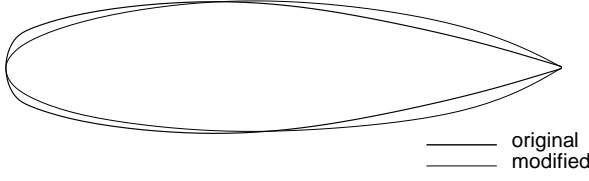
Figure 16: Shape of the modified airfoils for the untwisted wing.
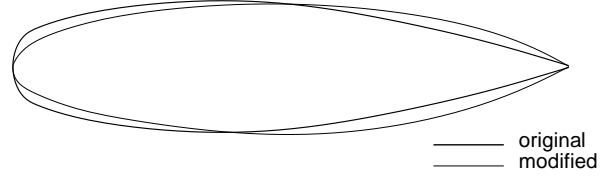
Figure 17: Shape of the modified airfoils for the twisted wing.

problem is hence:

$$
\left\{
\begin{array}{ll}
obj_1 = c_D/c_L^2 & \\[2mm]
obj_2 = (c_M + 0.13)^2 & \left.\right\} @M = 0.84, c_L = 0.3 \\[2mm]
obj_3 = c_D/c_L^2 & \left.\right\} @M = 0.90, c_L = 0.15
\end{array}
\right.
\tag{8}
$$

The geometry is represented using the same modification functions than the previous case (12 design variables). Furthermore, the same geometric constraints on thickness, leading edge radius and trailing edge angle are imposed.

Table 6 reports the parameter setting used for the genetic algorithm.

Variables encoding	8 bit
Selection	3 steps R. W.
	(20% from Pareto front)
Crossover	E.I.R., $p_c = 1$
Mutation	word level, $p_m = 0.05$
Population size	48
Generations	32

Table 6: genetic algorithm parameters used for the three-objective wing section design.

Figure 23 shows the obtained Pareto front with the selected individual evidenced. The third objective is here evidenced using a color scale, but it clear that when the number of objectives increases, it becomes very difficult to visualize the Pareto front in an intuitive way.

Figures 24 and 25 report the drag rise curves of the selected element at $c_L = 0.3$ and $c_L = 0.15$ respectively. Finally, figure 26 reports the Mach maps comparison between the original M6 wing and the wing selected from the front at the two design points.
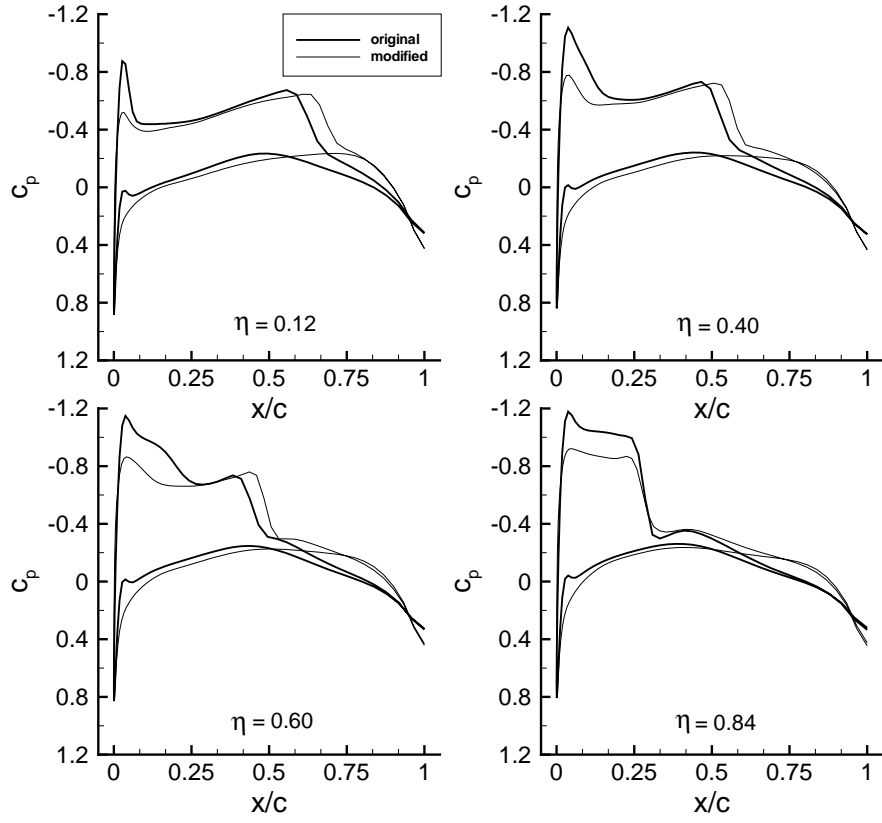
Figure 18: Pressure coefficient distributions on the original and optimized (untwisted) wings, with l.e. radius constraint.
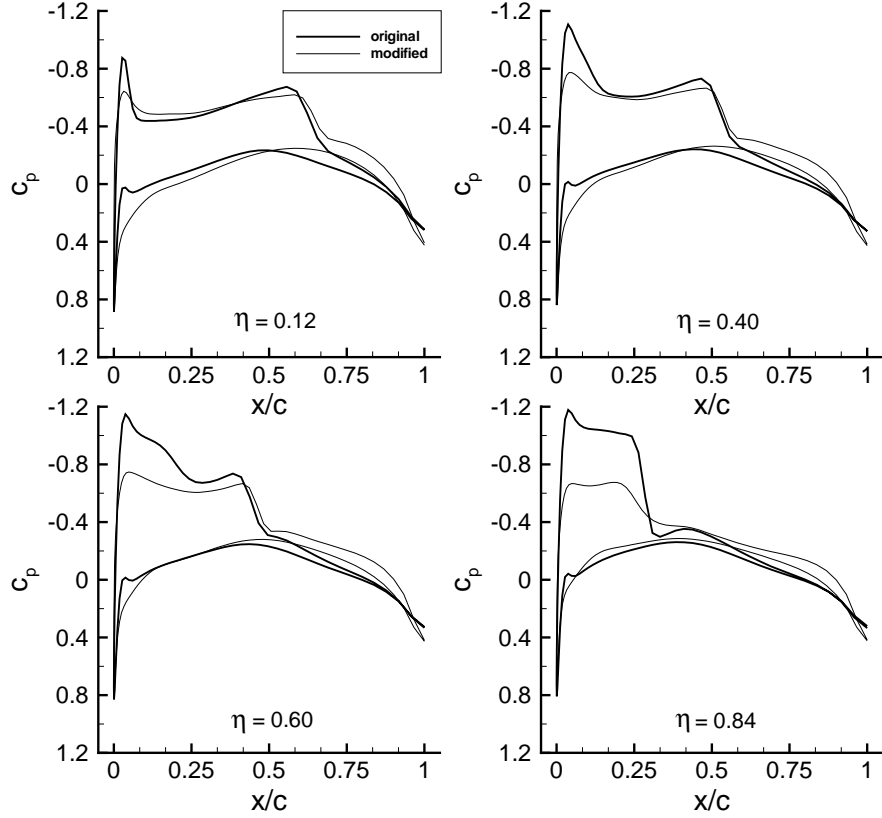

Figure 19: Pressure coefficient distributions on the original and optimized (twisted) wings, with l.e. radius constraint.
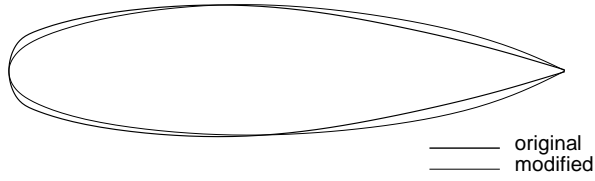
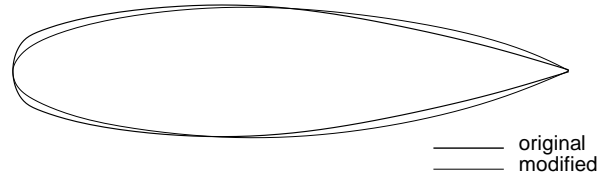Figure 20: Shape of the modified airfoils for the untwisted wing, with l.e. radius constraint.

Figure 21: Shape of the modified airfoils for the twisted wing, with l.e. radius constraint.

design problem #1

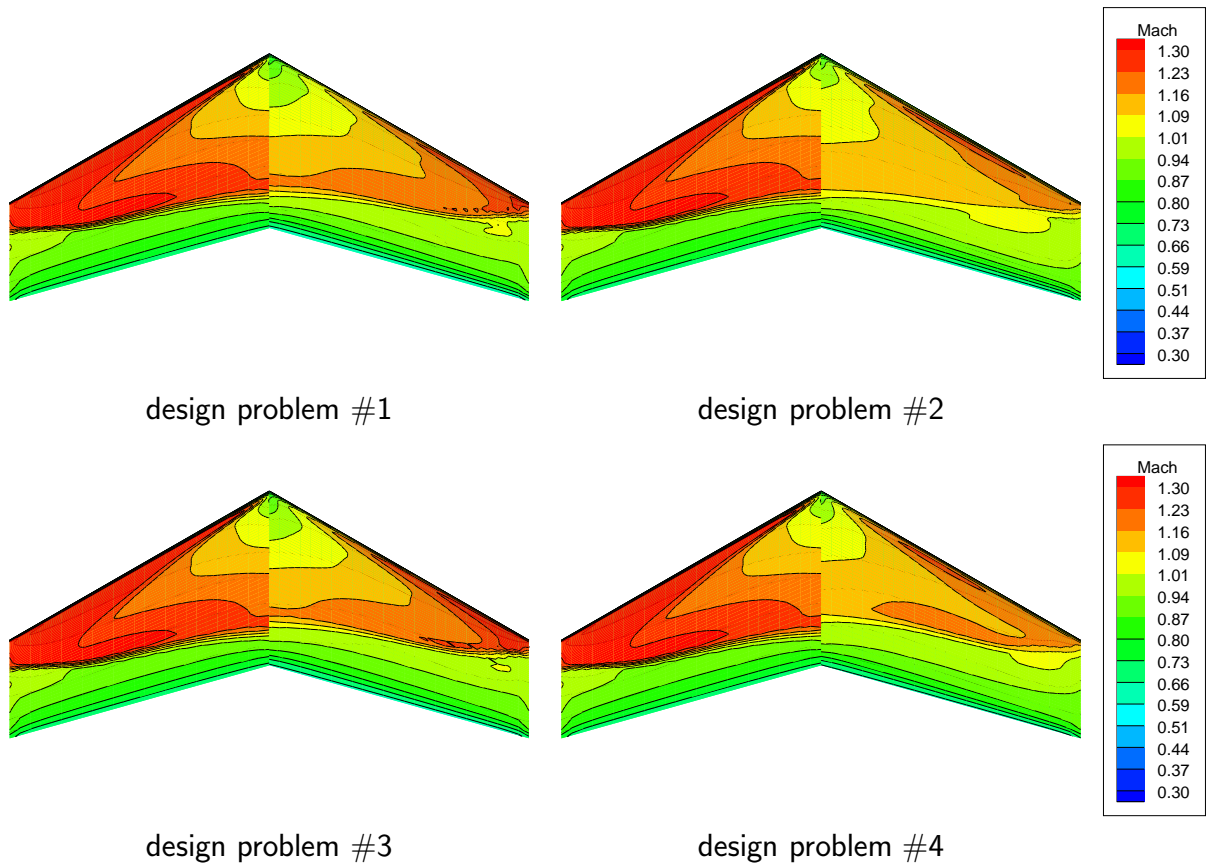design problem #2

design problem #3

design problem #4

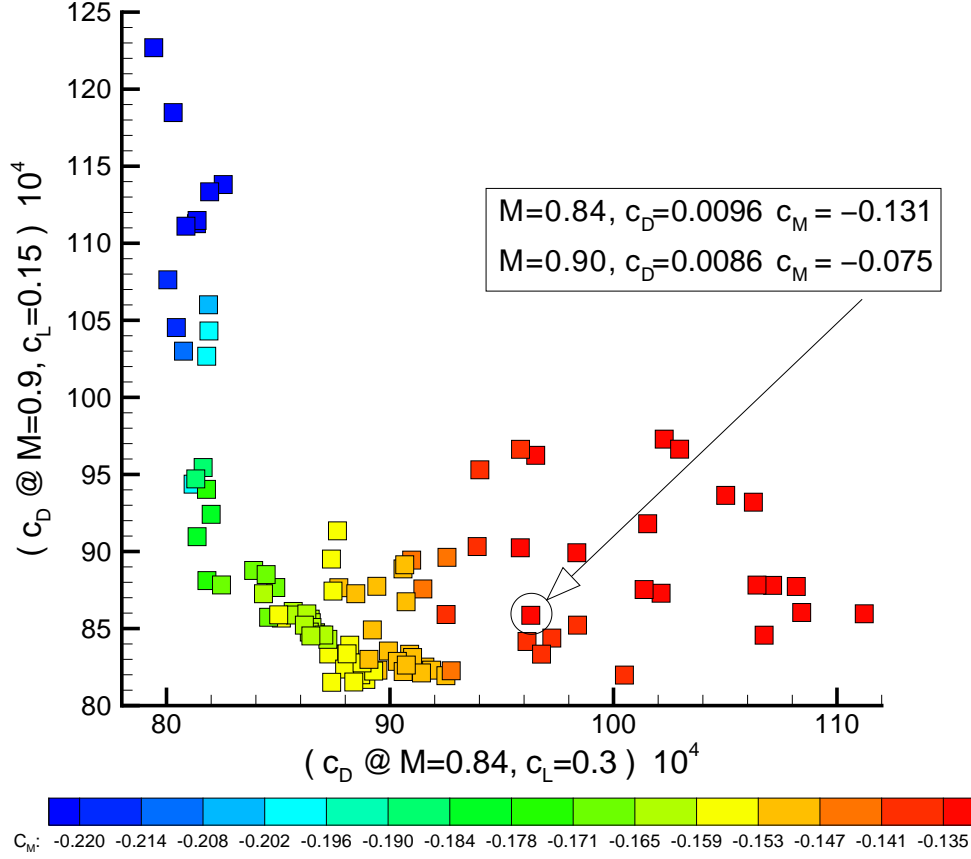Figure 22: Mach number distribution on the original (left) and optimized (right) wings.

Figure 23: Pareto front for the three-objective wing section design problem.

6 Conclusions

Multiple objective optimization is a powerful tool for aerodynamic design problems, and, in general, for multidisciplinary design and optimization tasks. Genetic algorithms offer unparalleled flexibility in the implementation of multi-objective optimization procedures. Furthermore, unlike the single-objective case, their computational efficiency compares favorably with more traditional approaches. Nevertheless it is of great interest the development of hybrid methods as they can significantly improve both the quality of the Pareto fronts developed, and the computational efficiency of the optimization procedure.

The main advantage of having a non-dominated set of solutions is that the designer can make the choice introducing an a posteriori criterion. However this advantage rapidly vanishes when the number of objective increases, unless some kind of automated assistance in the choice of the solution is introduced. Some techniques for assisting the decision maker in picking the best compromise solution may be found in [13].

References

[1] T. E. Labrujère, "Residual-correction type and related computational methods for aerodynamic design", in *Optimum Design Methods for Aerodynamics*, AGARD-R-803, AGARD, Nov. 1994.
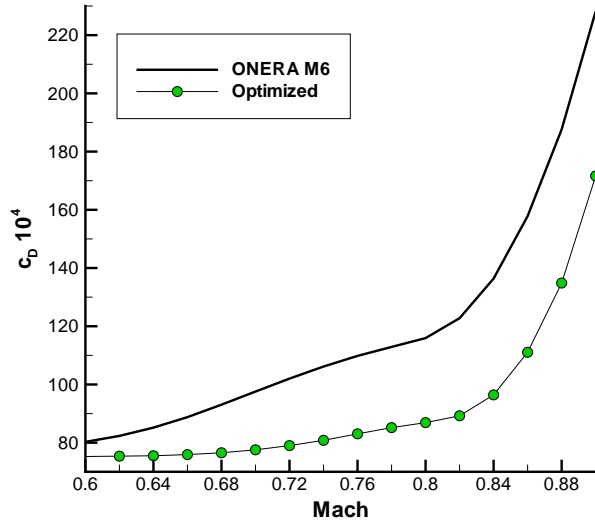
Figure 24: Three-objective wing design: drag rise curve of the selected element at $C_L = 0.3$.

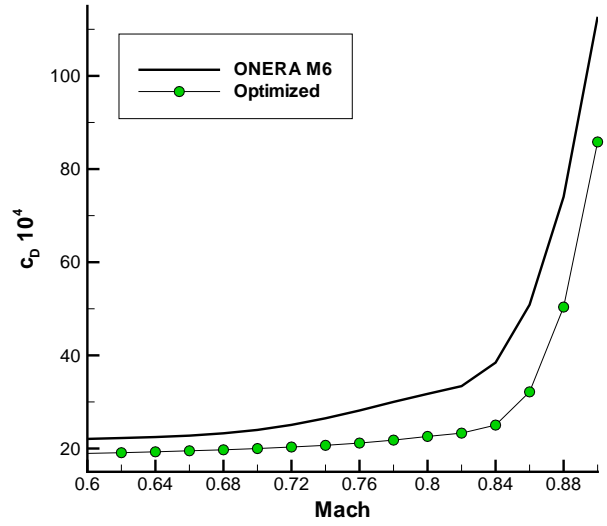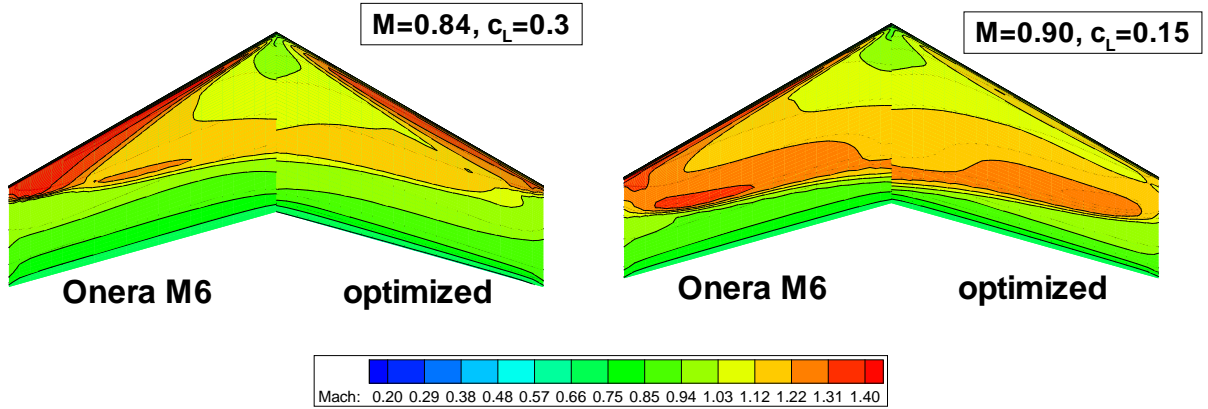Figure 25: Three-objective wing design: drag rise curve of the selected element at $C_L = 0.15$.

Figure 26: Three-objective wing design: Mach map comparison.

[2] F. T. Lynch, "Commercial Transports - Aerodynamic Design for Cruise Performance Efficiency", in Nixon D., editor, *Transonic Perspective Symposium, Progress in Aeronautics and Astronautics*, AIAA, New York, 1982, pp. 81–147.

[3] A. M. O. Smith, "High-Lift Aerodynamics", *Journal of Aircraft*, Vol. 12, No. 6, 1975, pp. 501–530.

[4] K. Deb, "Evolutionary Algorithms for Multi-Criterion Optimization in Engineering Design", in Miettinen K. et al., editors, *Evolutionary Algorithms in Engineering and Computer Science*, Wiley, England, May 1999, pp. 135–161.

[5] V. Chankong, and Y. Y. Haimes, *Multiobjective decision making: theory and methodology*, North Holland series in system science and engineering; 8, North Holland, New York, 1983.

[6] D. Quagliarella, and A. Vicini, "Coupling Genetic Algorithms and Gradient Based Optimization Techniques", in Quagliarella D. et al., editors, *Genetic Algorithms and Evolution Strategies in Engineering and Computer Science*, John Wiley & Sons Ltd., England, Nov. 1997, pp. 289–309.

[7] D. E. Goldberg, *Genetic Algorithms in Search, Optimization and Machine Learning*, Addison-Wesley, Reading, Massachusetts, Jan. 1989.

[8] K. Deb, "Multi-objective Genetic Algorithms: Problem Difficulties and Construction of Test Problems", *Evolutionary Computation*, Vol. 7, No. 3, 1999, pp. 205–230.

[9] A. Vicini, and D. Quagliarella, "Inverse and Direct Airfoil Design Using a Multiobjective Genetic Algorithm", *AIAA Journal*, Vol. 35, No. 9, Sep. 1997, pp. 1499–1505.

[10] M. Drela, "Newton solution of coupled viscous/inviscid multielement airfoil flows", in *AIAA, Fluid Dynamics, Plasma Dynamics and Lasers Conference*, AIAA Paper 90-1470, American Institute of Aeronautics and Astronautics (AIAA), Seattle, WA, June 1990.

[11] V. Schmitt, and F. Charpin, "Pressure distributions on the ONERA M6 wing at transonic Mach numbers", in *Experimental data base for computer program assessment*, AGARD AR-138, Paper B1, AGARD, May 1979.

[12] E. Torenbeek, "Development and Application of a Comprehensive, Design-Sensitive Weight Prediction Method for Wing Structures of Transport Category Aircraft", Technical Report LR-693, TU Delft, Sep. 1992.

[13] R. L. Keeney, and H. Raiffa, *Decisions With Multiple Objectives: Preferences and Value Tradeoffs*, Cambridge University Press, 1993.